NeuroImage **13,** 623–631 (2001)
doi:10.1006/nimg.2000.0734, available online at http://www.idealibrary.com on IDEAL®

Voxel-Based Morphometry of Herpes Simplex Encephalitis

Darren R. Gitelman,* John Ashburner,† Karl J. Friston,† Lorraine K. Tyler,‡ and Cathy J. Price†

*Cognitive Neurology and Alzheimer's Disease Center, Department of Neurology and Department of Radiology, Northwestern University Medical School, Chicago V.A. Healthcare System, Lakeside Division, Chicago, Illinois 60611; †Functional Imaging Laboratory, University College, London, United Kingdom; and ‡Department of Experimental Psychology, University of Cambridge, Cambridge, United Kingdom

Received August 22, 2000; published online February 13, 2001

Voxel-based morphometry (VBM) is a powerful tool for analyzing changes in gray or white matter density of the brain. By using an automated segmentation procedure and standardized parametric statistics it avoids biases inherent in operator-dependent morphological operations (J. Ashburner and K. J. Friston, 2000, *NeuroImage* 11, 805–821). Since its introduction in 1995, VBM has been used to examine anatomical changes in a variety of diseases associated with neurologic and psychiatric dysfunction. Given the power of this technique for discerning subtle anatomical changes, we wanted to assess its performance on brains with gross structural abnormalities. Such results could have implications regarding the difficulties to be faced when examining other types of distorted brains (e.g., brains with changes due to degenerative disease). This report describes the use of VBM for examining individual and group changes in gray matter concentration in five patients who had recovered from herpes simplex encephalitis (HSE) compared with age- and sex-matched controls. Because HSE tends to affect a specific set of brain regions we thought that this would (1) provide an opportunity to assess the anatomical face validity of VBM, (2) allow us to assess the problems of this technique when used on distorted brains, and (3) provide an *in vivo* demonstration of the gray matter changes due to HSE. We found that, despite problems in normalizing and segmenting these severely distorted brains, VBM was able to identify correctly a number of the regional gray matter abnormalities in HSE. The results, while consistent with the well-known histopathology of the disease, also demonstrate potential difficulties with this method.

INTRODUCTION

Morphometric analyses of brain anatomy date back over a century, but it is only within the past two decades that advances in imaging and computer technology have made this technique practical for examining large numbers of subjects with a variety of disorders. The methods used for morphometry can be broadly divided into label-based and non-label-based approaches. In the former, changes are measured with respect to operator-defined regions of interest (ROI) (Castellanos *et al.*, 1996; Filipek *et al.*, 1989; Jack *et al.*, 1999). The latter approach uses techniques such as voxel-based morphometry (VBM) (Ashburner and Friston, 2000) or analogous probabilistic methods (Thompson *et al.*, 1997), which do not require the *a priori* selection of ROIs. The potential advantages of the non-label-based methods are: (a) avoidance of operator bias in ROI definition (local bias), (b) quantification of features which are difficult to apprehend by inspection alone, and (c) comprehensive and simultaneous assessment of global brain anatomical changes which are not restricted (or blinded) by the selection of prespecified ROIs (global bias).

In the past few years, methods such as VBM have been increasingly utilized because of their comprehensive approach and their ability to identify (potentially) unsuspected alterations in brain anatomy. The technique has been used to reveal changes in gray or white matter in studies of schizophrenia (Wright *et al.*, 1995), developmental and congenital disorders (Abell *et al.*, 1999; Sowell *et al.*, 1999; Woermann *et al.*, 1999), Kallman's syndrome (Krams *et al.*, 1999), and even cluster headache (May *et al.*, 1999).

We applied VBM to five patients with a history of herpes simplex encephalitis (HSE). In humans, herpes simplex encephalitis is the most common of the viral encephalitides. The necrotizing form of the infection is both fulminating and devastating, resulting in death in over 28%, and moderate to severe disability in over 50%, of those affected despite the use of specific antiviral therapy (e.g., acyclovir) (McGrath *et al.*, 1997; Whitley, 1990).

Pathological studies of HSE have shown predominant viral-related damage in limbic and paralimbic regions of the brain, including the temporal lobes (hippocampal formation, amygdala, parahippocampal gyrus, and perirhinal cortex), orbitofrontal cortex, insula, and cingulate gyri (Damasio and Van Hoesen, 1985;

1053-8119/01 $35.00

TABLE 1

Demographics of Participants

Patient	Age of patient	Year of diagnosis	Age of controls	Gender
JH	33	1982	31.1 ± 0.98	Female
RC	38	1992	37.9 ± 2.03	Male
JBR	41	1980	43.7 ± 1.16	Male
YW	56	1993	53.9 ± 1.20	Female
JC	71	1994	65.6 ± 5.68	Female

Kennedy *et al.,* 1988; MacCallum *et al.,* 1973). Damage can be remarkably segregated, for example involving the anterior cingulate gyrus but not the adjacent posterior cingulate gyrus, corpus callosum, or supplementary motor cortex (Damasio and Van Hoesen, 1985). However, in cases with extensive necrosis the inflammatory response can damage regions outside of the limbic system such as the parietal and occipital lobes (Miller *et al.,* 1966). Infrequently, involvement of the brain stem and upper pons has also been seen (Rose *et al.,* 1992). The defined anatomic predilection of the herpes simplex virus for the limbic system allowed us to evaluate VBM under specified structural constraints.

METHODS

Subjects

Five patients with a history of HSE based on various standard clinical diagnostic measures (including EEG, changes on neuroimaging studies, and virological studies) underwent scanning for this study. Five normal comparison groups consisted of 10 subjects for each patient. The reason for assigning each patient his or her own control group was twofold: (1) to allow specific matching on age, sex, and handedness criteria and (2) to permit us to make inferences about regionally specific differences common to all patients as the inferences pertaining to each patient were then based on independent data. The scans for the control subjects were obtained from a database of scans at the Wellcome Department of Cognitive Neurology. These scans had been acquired over the past 3 years as the standard anatomic scan during each subject's participation in a variety of other functional imaging studies. Table 1 gives the basic demographic characteristics of the patient and control groups. HSE patients also underwent extensive neuropsychological testing, and these results will be reported in a subsequent study. All participants signed informed consent, and the study proceeded as approved by the local ethics committee.

MRI Scanning and VBM Analysis

A 2-T MRI scanner (Siemens Magnetom Vision, Erlangen, Germany) was used to acquire the anatomical volume images (TR/TE/IT 500/4/600 ms, flip angle 21°, matrix 256 × 224, 1 × 1 × 1.5-mm^3 voxels) in all patients and controls. The same scanner was used for all subjects. All image processing and analytical operations were performed within SPM99 (Welcome Department of Cognitive Neurology, London, UK) running under Matlab (Mathworks, Sherborn, MA). Each anatomical scan was realigned and normalized into a standardized space (ICBM) that approximates the space defined in the atlas of Talairach and Tournoux (1988). Subjects' brains were not masked during normalization, in order to allow the calculations to be informed by the shape of skull as well as the brain. This was necessary to provide a better estimate of gross brain shape as a consequence of the large areas of temporal lobe abnormality in the HSE patients. Both linear and nonlinear components were used in the normalization (7 × 8 × 7 nonlinear basis functions), although the nonlinear deformation fields were constrained by using a regularization scheme in order to prevent unlikely warping of the normalized images (Ashburner and Friston, 2000). As noted by Ashburner and Friston (2000), this normalization procedure is not expected to match cortical features precisely, otherwise differences between brains would be rendered inestimable with the VBM procedure. Instead, the procedure corrects for global shape differences such that changes in gray matter density are comparable for generally equivalent brain regions across the subject groups.

Following normalization, the images were segmented. The segmentation procedure in SPM99 utilizes a modified mixture model cluster analysis technique to partition the brain into gray matter, white matter, CSF, and scalp. In brief, the technique operates by comparing each brain voxel with voxels from a set of similarly normalized prior probability images. The probability images specify the likelihood that each voxel belongs to one of the aforementioned tissue classes (Evans *et al.,* 1992, 1993, 1994). The actual assignment of voxels to a particular tissue class is then determined iteratively depending on the mean and variance of the developing tissue clusters for the brain being analyzed (Ashburner and Friston, 2000). As a further processing step, the resulting gray matter probability images were multiplied by the Jacobian determinants of the deformation fields defined during normalization. This step has the effect of transforming gray matter per unit volume in normalized space to a density measure in native space[1] (Ashburner and Friston, 2000). The images are finally smoothed with a

[1] This step represents an optional refinement to the typical sequence of procedures used in VBM. By adjusting the relative concentration of gray matter for the regional expansion or contraction due to the nonlinear normalization field, the analysis is rendered more sensitive to absolute gray matter volume differences (Ashburner and Friston, 2000).

12-mm Gaussian kernel. Smoothing the segmented images is critical because it transforms the data from a high-resolution probabilistic map of gray matter location, into a low-resolution image of the relative amount of gray matter under the smoothing kernel. In other words, the smoothing is equivalent to a convolution operator, which has the effect of turning voxel values into a metric reflecting the local tissue composition. Furthermore, through the central limit theorem, smoothing results in the voxel values being more parametrically distributed, allowing the use of standard parametric statistics to make inferences about changes in gray matter concentration or density.

Statistical Analysis

The design matrix for our statistical model represented each patient and control group in a separable fashion. Contrasts were then specified comparing each patient with their respective controls. This allowed us to report the results as a series of case studies. In addition, because of the separable design matrix all contrasts were orthogonal, allowing us to combine the contrasts in a conjunction analysis to identify regions of common abnormality across all patients. The design matrix also included a covariate that treated global differences in gray matter as a confound. By covarying for global changes the results pertain to regionally specific differences in gray matter rather than global measures of atrophy.

Significance was assigned to the resulting t fields using the theory of Gaussian random fields (Friston *et al.*, 1995; Worsley *et al.*, 1996). The resulting statistical map was thresholded at $P < 0.05$ corrected for multiple comparisons across the volume.

RESULTS

Figures 1A–1E show representative results of the spatial normalization for each subject in comparison with the mean image of their corresponding control group. Although the large areas of temporal lobe necrosis in patient JH (best seen in Fig. 1A, top left coronal image) interfered with normalization, the overall brain shapes are comparable between the HSE and the normal subject groups. Nevertheless, differences do remain between the two groups, and the ventricles, in particular, are clearly larger in the HSE group. Adding more basis functions to the nonlinear deformations ($10 \times 12 \times 10$) or reducing the smoothness of the deformation fields (to allow fitting of greater deviations from the template) did not improve the outcome and resulted in increasing distortions. Unfortunately there is no simple metric for documenting the "goodness of fit" of the normalization procedure. While the normalization algorithm does provide measures of the least-squares fit and deformation field smoothness, these results do not indicate, in isolation, how well the algorithm has performed. Therefore this report and all previous studies utilizing VBM have relied on visual assessments of the overall brain shape among subject groups (Abell *et al.*, 1999; Ashburner and Friston, 2000; Krams *et al.*, 1999; May *et al.*, 1999; Mummery *et al.*, 2000; Sowell *et al.*, 1999; Wright *et al.*, 1995). The check registration function in SPM99 was used to ensure that there was correspondence between the patients and the controls for major landmarks such as the AC and PC points, frontal and occipital poles, and left and right temporal extremes. This function visually demonstrates corresponding points on the series of selected images. The graphical output of this function is illustrated in Fig. 1 and demonstrates that the images showed good general correspondence (e.g., see the cross hairs).

Segmentation performance was excellent in the normal subject group. Figure 2 shows a slice from the smoothed segmented gray matter maps for a patient (bottom) and one normal subject from a matching group (top) on the left and their corresponding anatomical images on the right. The smoothed gray matter maps represent the "gray matter density" images that are entered into the statistical analysis. In the patient images, the segmenting algorithm also performed well despite the evident distortions. Subtle problems were seen, however, for areas such as the caudate nucleus (Fig. 2, arrows). In this patient's scan, the caudate did not match precisely with its location on the prior probability map because of ventricular enlargement. Thus the amount of caudate gray matter in the patient group was mildly underestimated and displaced from its true position. Note that the cross hairs should be on the same anatomical structure in all images if normalization was perfect.

Figure 3 shows the results of VBM. All colored areas represent significantly reduced gray matter concentration in the patients compared with the corresponding control group, based on a height threshold of $P < 0.05$ corrected for multiple comparisons. The color for each patient in Fig. 3A corresponds to colors in the combined map shown in Fig. 3B. Figure 3A shows representative sections from each patient with areas of significantly reduced gray matter overlaid on each patient's own brain. In general, most of the abnormal gray matter regions do not represent subtle changes. Figure 3B shows the gray matter abnormalities from each patient combined and overlaid on an average of all the normal subject brains. Anatomical structures are indicated. As illustrated in Figs. 3A and 3B, the areas of most prominent gray matter abnormality were in the temporal lobes, including the anterior aspects of the lateral temporal cortex, the temporal poles, and the medial temporal cortex including the amygdala, hippocampus, and entorhinal cortex. Dorsally these areas of abnormality involved the insula extensively. Abnormalities were seen medially overlying the subcallosal gyrus and the medial aspects of the nuclei accumbens. One pa-

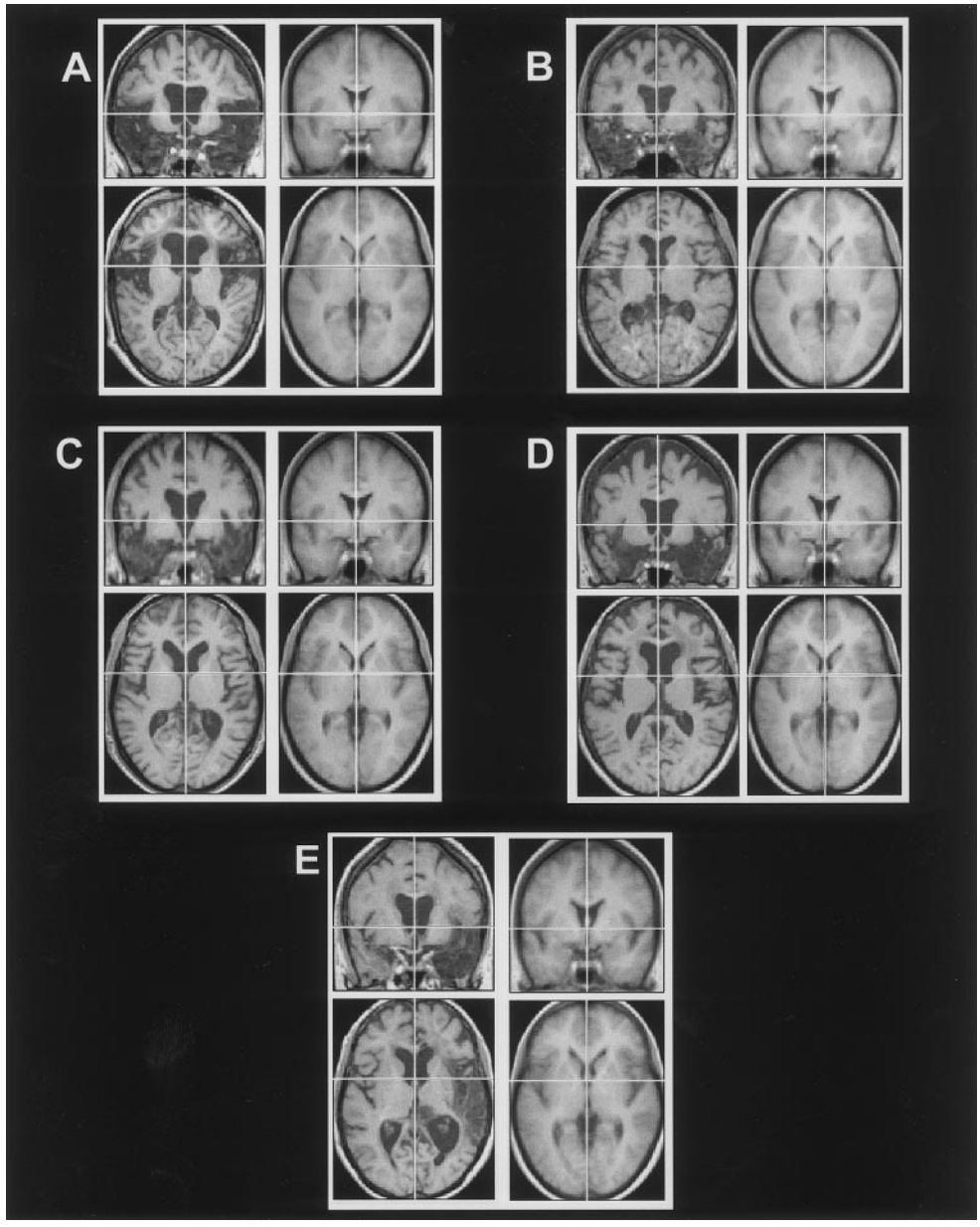

FIG. 1. Representative slices of each patient's brain and the mean of each corresponding control group demonstrating results of spatial normalization (A—JH, B—RC, C—JBR, D—YW, E—JC). The images are oriented with the left side of the head on the left side of each image in this and in all subsequent figures.

tient (YW) also had changes involving the posterior parietal cortex and the dorsal premotor region (not shown in the figure).

Conjunction analysis of the abnormalities in all patients demonstrates the areas of gray matter change that were common across the patients. This comparison (Fig. 3C) confirmed the shared abnormalities in the medial temporal lobes (amygdala and hippocampus), temporal pole and anterior lateral temporal cortex, gyrus rectus (subcallosal area), and insula. The areas of abnormality also overlap in what appears to be the ventricles. However, it is not possible to determine whether this truly represents gray matter changes in medial caudate nuclei or more likely the comparison of caudate gray matter in the control group with the ventricles in the patients (because the caudate nuclei may have been displaced due to ventricular enlargement in the patients).

DISCUSSION

Voxel-based morphometry was used to demonstrate extensive limbic and paralimbic anatomical changes in

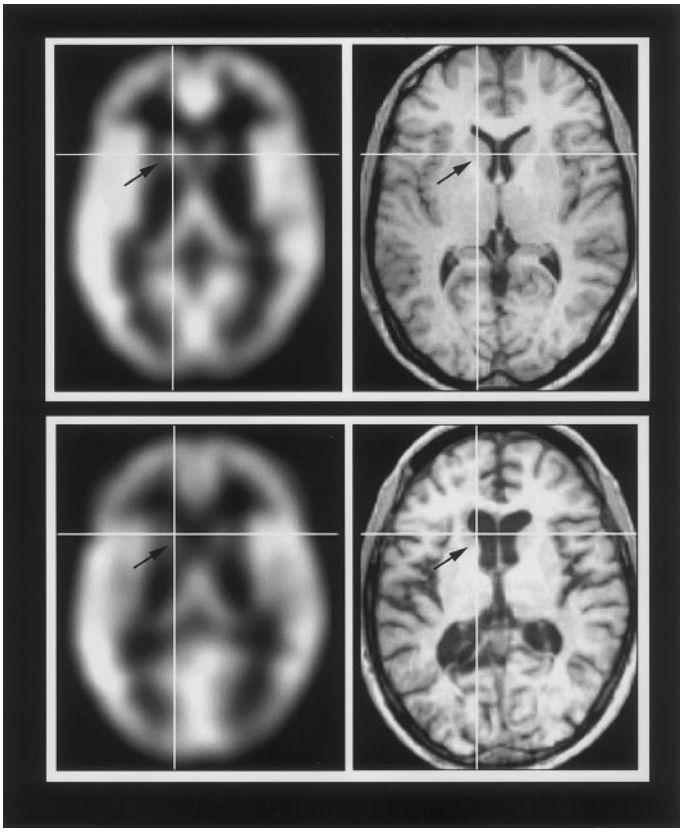

FIG. 2. Smoothed gray matter segments and corresponding anatomical slices from one patient (bottom) and one member of the corresponding control group (top). The arrow points to the location of the left caudate nucleus in all sections. Note that the estimation of caudate gray matter is reduced in the patient (fewer white pixels at the arrow in the lower left image) even though the patient clearly still has caudate nucleus present on the anatomical image (lower right). In this case, slight mismatches between the position of the caudate in the normalized patient image and its position in the probability map interfered with segmentation.

patients with a history of severe herpes simplex encephalitis. The results were highly consistent with many of the pathological changes that have been previously documented for this disorder (Damasio and Van Hoesen, 1985; Dinn, 1979; Dudgeon, 1969; Kennedy *et al.*, 1988). However, it is important to point out that our findings do not demonstrate every possible area of involvement in HSE, and they illustrate possible areas of caution when applying this methodology to other disorders.

We chose to study HSE because it is known to cause relatively specific, albeit expansive, lesions that are primarily confined to the limbic lobe of the brain. The limbic lobe contains many of the phylogenetically oldest areas of the cerebrum and can be divided into the limbic cortex and paralimbic association cortex. The limbic cortex consists of the hippocampus, subiculum, prepiriform area, amygdala, and periamygdaloid complex. Paralimbic association cortex includes the gyrus rectus (subcallosal area) and cingulate gyri, retrosplenial region, parahippocampal gyrus (entorhinal cortex), perirhinal area, and insula (Duvernoy *et al.*, 1999). These regions share close anatomic connectivity (Mesulam, 1985) and may also possess shared immunological markers, making them a common target of the herpes simplex virus. Previous pathological studies of HSE have almost uniformly shown injury and the presence of viral antigens in various regions of limbic and paralimbic cortex (Dinn, 1979; Esiri, 1982). Although presence of viral antigen has been documented in extralimbic areas, including the isocortical motor strip (Damasio and Van Hoesen, 1985), postcentral cortex (Esiri, 1982), and brain-stem structures of the pons and medulla (Esiri, 1982), these regions rarely show necrotic changes.

All five patients in the current analysis showed abnormal gray matter density in various regions of limbic and paralimbic cortex, but the degree and pattern of involvement varied. It is notable that the areas of abnormality were asymmetric in individuals and over the group as a whole. Prior pathological studies have also demonstrated that asymmetrical lesions are a common finding in HSE (MacCallum *et al.*, 1973). However, the particular right-sided asymmetry in our group of HSE patients is not a feature of prior pathological reports and may represent bias due to the restricted number of patients in the current analysis (Damasio and Van Hoesen, 1985; Kennedy *et al.*, 1988; MacCallum *et al.*, 1973). While the lesions identified by VBM were extensive they appeared to reflect actual lesions seen on MRI. Furthermore the identified areas of gray matter abnormality did not overlap normal cortex. Thus despite the obvious anatomical distortions induced by this disease, the areas of significant gray matter abnormality do not appear to be arbitrarily associated with other parts of cortex (i.e., abnormalities were not seen overlying dorsolateral prefrontal cortex).

Certain regions of limbic cortex such as the cingulate gyrus do not show any gray matter abnormalities in the current analysis, although their involvement has been noted in previous pathological studies of HSE (Damasio and Van Hoesen, 1985). Review of the raw patient images in the current study did not show obvious lesions in the region of the cingulate gyrus, although by visual inspection patients did show more atrophy of this region that did not reach statistical significance. While the absence of significant gray matter abnormality in this area may represent a true negative in this group of five patients, other causes of reduced sensitivity for this technique include errors in normalization and segmentation and the effects of spatial smoothing. Each of these factors will be discussed in turn.

Generally, VBM is applied to patients who have normal overall brain shapes. The idea is then to use spatial normalization to remove (relatively minor) posi-

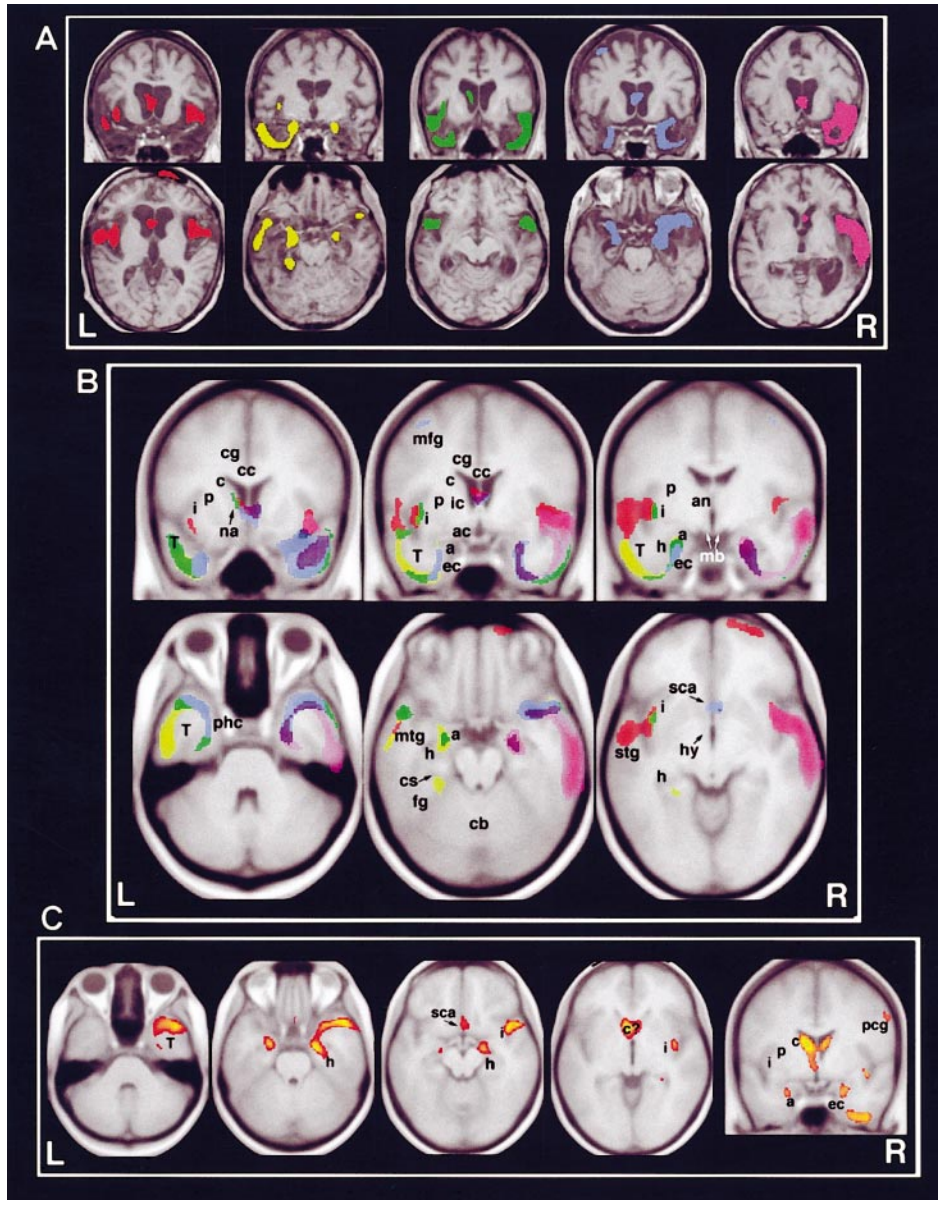

FIG. 3. Sections showing areas of gray matter deficiency compared with controls, $P < 0.05$ corrected for multiple comparisons. The colors in A and B correspond to each of the five patients. (A) Representative results from each patient overlaid on his or her own brain. Note consistent involvement of temporal lobe and insular/perisylvian structures. The images are ordered from left to right corresponding to the individual patients as in Table 1. (B) Results from each patient combined and overlaid on the average of the control brains. Anatomical structures are indicated (see key below). (C) Conjunction analysis showing areas of common gray matter reduction across the patient group. Key: a, amygdala; ac, anterior commissure; an, anterior nucleus of thalamus; c, caudate nucleus; c?, caudate versus ventricular abnormality; cb, cerebellum; cc, corpus callosum; cg, cingulate gyrus; cs, collateral sulcus; ec, entorhinal cortex; fg, fusiform gyrus; gr, gyrus rectus; h, hippocampus; hy, hypothalamus; i, insula; ic, internal capsule; mb, mamillary bodies; mfg, middle frontal gyrus; mtg, middle temporal gyrus; na, nucleus accumbens; p, pulvinar; pcg, precentral gyrus; sca, subcallosal gyrus; stg, superior temporal gyrus; T, temporal lobe.

tional differences up to a certain spatial scale such that any residual differences can be accounted for only by the local macroscopic structure of the brain. Clearly, this assumption is violated if substantial macroscopic differences persist following spatial normalization at a spatial scale that is greater than the smoothing kernel employed. Errors in normalization can then affect the VBM result directly or can represent an interaction with the segmentation component.

Figure 1 illustrates variations in normalization results among the group of subjects. As expected, patients with more pronounced lesions appeared to show more deviation from their respective controls (Fig. 1A). Several strategies have been described for dealing with

gross brain lesions. These include masking out abnormal areas of cortex to reduce their influence on the calculations, using signal from the skull and other tissues outside the brain to constrain the boundaries of normalization, smoothing the nonlinear deformation fields (to avoid excessive displacements caused by warping normal brain into areas of abnormality), and using other basis functions or minimization algorithms for matching the subject and template brains (Ashburner and Friston, 2000; Fox *et al.*, 1999; Thompson *et al.*, 1997). In the present analysis we chose to constrain the normalization by using the entire head and by constraining (smoothing) the deformation fields, since these measures are easily implemented in SPM99. While these choices produced a reasonable result (Fig. 1), we recognize that there are other approaches to the difficult question of normalizing highly abnormal brains. The lack of an absolute metric for the goodness of normalization has been noted and represents one area of future research.

Segmentation separates the brain into gray matter, white matter, and other tissue images. The algorithm in SPM99 assigns each voxel to a particular tissue class by combining information regarding the voxel's intensity value, the classification of that same voxel in the probability images, and the mean and standard deviation of each tissue class' voxel values based on the brain being analyzed. Voxels in abnormal brains therefore can be misclassified by virtue of having abnormal values, by their misalignment with the template image, or because the mean and variance of the voxel values for a tissue class have been affected by the inclusion in that class of abnormal or misspecified voxels.

For example, in our analyses differences between patients and controls were found overlying the heads of the caudate nuclei. Normally, one would infer that there was reduced gray matter centered on the caudate in patients with HSE. However, in the context of ventricular enlargement, this regionally specific difference may be simply attributable to an alteration in the caudate's position, and a consequent inability to classify some of its voxels as gray matter. The interaction with the segmentation procedure is possible because the prior information about the probability of being gray matter is based upon templates that conform to normal anatomy. This does not invalidate the inferences made with VBM, but speaks to a qualification of any simplistic interpretation in terms of changes in the composition of a given brain structure. Therefore, although the caudate nuclei and surrounding brain structures are abnormal in HSE, this may not be due to reduced gray matter density per se, but to a displacement of brain structures that the spatial normalization could not model.

In light of the possible interactions between normalization and segmentation, we note that it is important to examine any detected differences with respect to both the normal and the abnormal subject brains. In our subject groups, the changes in the ventricular system shown in Fig. 3 corresponded to the caudate nuclei in the normal group but the ventricles in the patient group. By referencing identified differences to each patient's brain and average brains of the normal subject groups, we were careful to assign anatomic differences to the proper structure.

With respect to potential inaccuracies induced by the spatial smoothing procedure, although this step does reduce the resolution of the gray matter images it is necessary to condition the data for the reasons noted under Methods. Moreover similar spatial smoothing kernels have been used in other VBM reports and have not interfered with the detection of relatively subtle gray matter differences (e.g., gray matter differences in the hypothalamus in cluster headache; May *et al.*, 1999).

Given the difficulties in normalizing the brains in this study, and the small number of patients, we were careful to report only voxels surviving a threshold of $P < 0.05$ corrected for multiple comparisons across the entire volume. Nevertheless, when comparing single subjects to a group there are still concerns that this design may increase the likelihood of violating the parametric assumptions regarding the distribution of the residuals and the approximation of the residuals to the true errors of the dataset. The reason for this is that the original partition images have a highly nonnormal density function; they are restricted to the range from 0 to 1 and generally have more mass at the extremes. Although spatial smoothing renders the distribution near normal by the central limit theorem, some nonnormality may persist. Usually this nonnormality can be discounted because the residuals are themselves a linear compound of the data (determined by the rows of the residual forming matrix), and the central limit theorem ensures normality. However, some residual forming matrices (e.g., those comparing one subject to a larger group) put most of the weight on the single subject. As a consequence, the *P* values may be inexact and therefore should be treated with a degree of caution. Increasing the numbers of subjects can reduce this potential bias. In addition, using both null contrasts on empirical data and simulated data, we have found that these designs have not resulted in an excess of false positives provided the smoothing kernel is at least 4 mm FWHM (Ashburner and Friston, unpublished data). Nevertheless, it is difficult to generalize statements about robustness to all situations, and careful interpretation and qualification of the results will always be important.

In summary, in patients with HSE, VBM was able to accurately detect gray matter abnormalities in limbic and paralimbic areas of cortex, consistent with previous pathologic descriptions of the disorder. This establishes the face validity of the technique and provides a dramatic illustration of the cortical lesions in this con-

dition. While the distorted brains in our analysis provide a special challenge, they also illustrate the importance of considering interactions between brain morphology and analytical methods. These interactions can confound any simple interpretation of VBM or other similar techniques. Comparable issues will have to be addressed when, for example, patients with dementia are compared to older control groups or when aging populations are compared to the young.

In terms of future work, there are a number of important extensions to pursue. First, it is important to resolve the ambiguity in interpretation of VBM results in the context of imprecise spatial normalization. One possible approach will entail the use of high dimensional spatial normalization routines as embodied by tensor-based morphometry, for example, which provides a detailed characterization of the local deformations that are required to map one brain to another. Other lines of work will harness the flexibility afforded by the general linear model in the context of voxel-based morphometry. In this paper we have simply reported categorical differences between patients and controls as a series of case studies and in terms of a conjunction analysis. A possible next step would be to make more refined inferences using parametric designs. For example, with a larger number of subjects, one can look for correlations with disease duration, behavioral or psychological indices, or other markers of pathophysiology. An interesting extension of this idea is to examine the progressive changes in structural pathology, using VBM, by looking for correlations over time (or over subjects) between the relative gray matter densities in different brain regions. This can be approached by looking for areas that covary significantly, in terms of gray matter density, with a region known to be implicated early in the pathophysiology of the disease (e.g., the medial temporal lobe). Areas that may not survive significance criteria, using categorical designs, may be revealed by this approach and may be expressed as coherent spatial modes of reduced gray matter density that are expressed over time within subject, or over a cohort of subjects with variable disease progression.

ACKNOWLEDGMENTS

This study was supported by NIA Grant K23 AG00940 to D.R.G., J.A., K.J.F., and C.J.P. were supported the Wellcome Trust, and L.K.T. was supported by the MRC.

REFERENCES

Abell, F., Krams, M., Ashburner, J., Passingham, R. E., Friston, K. J., Frackowiak, R. S. J., Happe, F., Frith, C. D., and Frith, U. 1999. The neuroanatomy of autism: A voxel based whole brain analysis of structural scans. *NeuroReport* **10:** 1647–1651.

Ashburner, J., and Friston, K. J. 2000. Voxel-based morphometry—The methods. *NeuroImage* **11:** 805–821.

Castellanos, F. X., Giedd, J. N., Hamburger, S. D., Marsh, W. L., and Rapoport, J. L. 1996. Brain morphometry in Tourette's syndrome: The influence of comorbid attention-deficit/hyperactivity disorder. *Neurology* **47:** 1581–1583.

Damasio, A. R., and Van Hoesen, G. W. 1985. The limbic system and the localisation of herpes simplex encephalitis. *J. Neurol. Neurosurg. Psychiatry* **48:** 297–301.

Dinn, J. J. 1979. Distribution of herpes simplex virus in acute necrotising encephalitis. *J. Pathol.* **129:** 135–138.

Dudgeon, J. A. 1969. Herpes encephalitis. II. Pathology of herpes encephalitis. *Postgraduate Med. J.* **45:** 386–391.

Duvernoy, H. M., Bourgouin, P., Cabanis, E. A., Cattin, F., Guyot, J., Iba-Zizen, M. T., Maeder, P., Parratte, B., Tatu, L., and Vuillier, F. 1999. *The Human Brain: Surface, Three-Dimensional Sectional Anatomy with MRI, and Blood Supply.* Springer-Verlag, Vienna/New York.

Esiri, M. M. 1982. Herpes simplex encephalitis: An immunohistological study of the distribution of viral antigen within the brain. *J. Neurol. Sci.* **54:** 209–226.

Evans, A. C., Collins, D. L., Mills, S. R., Brown, E. D., Kelly, R. L., and Peters, T. M. 1993. 3D statistical neuroanatomical models from 305 MRI volumes. In *Proc. IEEE Nucl. Sci. Symp. Med. Imag. Conf.*, pp. 1813–1817.

Evans, A. C., Collins, D. L., and Milner, B. 1992. An MRI-based stereotactic atlas from 250 young normal subjects. *Soc. Neurosci. Abstr.* **18:** 408.

Evans, A. C., Kamber, M., Collins, D. L., and MacDonald, D. 1994. An MRI-based probabilistic atlas of neuroanatomy. In *Magnetic Resonance Scanning and Epilepsy. NATO ASI Series A, Life Sciences* (S. Shorvon, D. Fish, F. Andermann, G. M. Bydder, and H. Stefan, Eds.), Vol. 264, pp. 263–274. Plenum, New York.

Filipek, P. A., Kennedy, D. N., Caviness, V. S., Jr., Rossnick, S. L., Spraggins, T. A., and Starewicz, P. M. 1989. Magnetic resonance imaging-based brain morphometry: Development and application to normal subjects. *Ann. Neurol.* **25:** 61–67.

Fox, N. C., Warrington, E. K., and Rossor, M. N. 1999. Serial magnetic resonance imaging of cerebral atrophy in preclinical Alzheimer's disease. *Lancet.* **353.**

Friston, K. J., Holmes, A. P., Worsley, K. J., Poline, J.-B., Frith, C. D., and Frackowiak, R. S. J. 1995. Statistical parametric maps in functional imaging: A general linear approach. *Hum. Brain Mapp.* **2:** 189–210.

Jack, C. R., Jr., Petersen, R. C., Xu, Y. C., O'Brien, P. C., Smith, G. E., Ivnik, R. J., Boeve, B. F., Waring, S. C., Tangalos, E. G., and Kokmen, E. 1999. Prediction of AD with MRI-based hippocampal volume in mild cognitive impairment. *Neurology* **52:** 1397–1403.

Kennedy, P. G. E., Adams, J. H., Graham, D. I., and Clements, G. B. 1988. A clinico-pathological study of herpes simplex encephalitis. *Neuropathol. Appl. Neurobiol.* **14:** 395–415.

Krams, M., Quinton, R., Ashburner, J., Friston, K. J., Frackowiak, R. S. J., Bouloux, P. M., and Passingham, R. E. 1999. Kallman's syndrome: Mirror movements associated with bilateral corticospinal tract hypertrophy. *Neurology* **52:** 816–822.

MacCallum, F. O., Adams, H., and Miller, D. 1973. Herpes simplex encephalitis: A clinical and pathological analysis of twenty-two cases. *Postgraduate Med. J.* **49:** 393–397.

May, A., Ashburner, J., Buchel, C., McGonigle, D. J., Friston, K. J., Frackowiak, R. S., and Goadsby, P. J. 1999. Correlation between structural and functional changes in brain in an idiopathic headache syndrome. *Nat. Med.* **5:** 836–838.

McGrath, N., Anderson, N. E., Croxson, M. C., and Powell, K. F. 1997. Herpes simplex encephalitis treated with acyclovir: Diagnosis and long term outcome. *J. Neurol. Neurosurg. Psychiatry* **63:** 321–326.

Mesulam, M.-M. 1985. Patterns in behavioral neuroanatomy: Association areas, the limbic system and hemispheric specialization. In *Principles of Behavioral Neurology* (M.-M. Mesulam, Ed.), pp. 1–58. Davis, Philadelphia.

Miller, J. K., Hesser, F., and Tompkins, V. N. 1966. Herpes simplex encephalitis. *Ann. Intern. Med.* **64:** 92–103.

Mummery, C. J., Patterson, K., Price, C. J., Ashburner, J., Frackowiak, R. S. J., and Hodges, J. R. 2000. A voxel-based morphometry study of semantic dementia: Relationship between temporal lobe atrophy and semantic memory. *Ann. Neurol.* **47:** 36–45.

Rose, J. W., Stroop, W. G., Matsuo, F., and Henkel, J. 1992. Atypical herpes simplex encephalitis: Clinical, virologic, and neuropathologic evaluation. *Neurology* **42:** 1809–1812.

Sowell, E. R., Thompson, P. M., Holmes, C. J., Batth, R., Jernigan, T. L., and Toga, A. W. 1999. Localizing age-related changes in brain structure between childhood and adolescence using statistical parametric mapping. *NeuroImage* **9:** 587–597.

Talairach, J., and Tournoux, P. 1988. *Co-planar Stereotaxic Atlas of the Human Brain.* Thieme, New York.

Thompson, P. M., MacDonald, D., Mega, M. S., Holmes, C. J., Evans, A. C., and Toga, A. W. 1997. Detection and mapping of abnormal brain structure with a probabilistic atlas of cortical surfaces. *J. Comput. Assisted Tomogr.* **21:** 567–581.

Whitley, R. J. 1990. Viral encephalitis. *N. Engl. J. Med.* **323:** 242–250.

Woermann, F. G., Free, S. L., Koepp, M. J., Ashburner, J., and Duncan, J. S. 1999. Voxel-by-voxel comparison of automatically segmented cerebral gray matter—A rater-independent comparison of structural MRI in patients with epilepsy. *NeuroImage* **10:** 373–384.

Worsley, K. J., Marrett, S., Neelin, P., Vandal, A. C., Friston, K. J., and Evans, A. C. 1996. A unified statistical approach for determining significant signals in images of cerebral activation. *Hum. Brain Mapp.* **4:** 58–73.

Wright, I. C., McGuire, P. K., Poline, J.-B., Travere, J. M., Murray, R. M., Frith, C. D., Frackowiak, R. S. J., and Friston, K. J. 1995. A voxel-based method for the statistical analysis of gray and white matter density applied to schizophrenia. *Hum. Brain Mapp.* **2:** 244–252.